Analyst

Cite this: *Analyst*, 2012, **137**, 3773

www.rsc.org/analyst

PAPER

Raman spectroscopy and imaging: applications in human breast cancer diagnosis

Beata Brozek-Pluska,*[a] Jacek Musial,[b] Radzislaw Kordek,[c] Elena Bailo,[d] Thomas Dieing[e] and Halina Abramczyk[f]

Received 30th November 2011, Accepted 5th June 2012
DOI: 10.1039/c2an16179f

The applications of spectroscopic methods in cancer detection open new possibilities in early stage diagnostics. Raman spectroscopy and Raman imaging represent novel and rapidly developing tools in cancer diagnosis. In the study described in this paper Raman spectroscopy has been employed to examine noncancerous and cancerous human breast tissues of the same patient. The most significant differences between noncancerous and cancerous tissues were found in regions characteristic for the vibrations of carotenoids, lipids and proteins. Particular attention was paid to the role played by unsaturated fatty acids in the differentiation between the noncancerous and the cancerous tissues. Comparison of Raman spectra of the noncancerous and the cancerous tissues with the spectra of oleic, linoleic, α-linolenic, γ-linolenic, docosahexaenoic and eicosapentaenoic acids has been presented. The role of sample preparation in the determination of cancer markers is also discussed in this study.

1. Introduction

The National Cancer Institute at the National Institute of Health in the USA estimates that throughout 2011 there were more than 200 000 new cases of breast cancer in women in the United States. At the same time there were over 39 000 mortal cases of breast cancer in the US. These data reflect world statistics, which prove that breast cancer is one of the most common types of cancers among women.

In the traditional approach cancer can be identified using different well established methods, such as computer tomography (CT), magnetic resonance imaging (MRI), positron emission tomography (PET), X-ray, ultrasound, biopsy and in the case of breast cancer also mammography or miraluma breast imaging was used. However, the preferred method for diagnosing breast cancer is histological analysis.

Presently a histological analysis, being the standard procedure for breast cancer diagnostics, can sometimes be inconvenient and time consuming, and in a number of cases leads to ambiguous results prone to human interpretations. Evidently this shows the need to develop new methods that would enable an unequivocal diagnosis within a short time. A number of groups have been working to utilize spectroscopic methods to study abnormalities in biological tissues.[1–6]

Over the past few years medical applications of Raman spectroscopy (RS) and Raman imaging (RI) have gone through rapid development, particularly in the area of fast diagnostic analysis. RS and RI cover a broad spectrum of diagnostic applications, including Alzheimer's disease and skin diseases, as well as analysis of body fluids.[7–10] However, the leading place is taken by cancer diagnosis. Current instrumentation has enabled a fast analysis of different cancer tissue samples including histological sections, bulk tissues and single cells.[11–13]

Alfano and coworkers were the first to look at the ability of Raman spectroscopy to distinguish noncancerous breast tissues from malignant ones.[14] Later, Redd[15] and coworkers demonstrated the advantages of NIR excitation in the context of breast cancer. Both groups saw closely similar results showing a decrease in lipid contributions in the spectra from infiltrating ductal carcinoma (IDC) samples, as well as an increase in the collagen contributions in benign and malignant samples. More recently, Feld and coworkers have presented an extensive work on using Raman spectroscopy for breast cancer diagnosis.[16] Stone and coworkers also demonstrated that the Raman spectroscopy technique has significant potential for probing the human body to provide complementary data in the early diagnosis of breast cancer.[17,18] Spectroscopic characterization of breast duct epithelia, the basis for understanding epithelium-derived breast tumors, was published by the Puppels group.[6]

[a]*Lodz University of Technology, Institute of Applied Radiation Chemistry, Laboratory of Laser Molecular Spectroscopy, Wroblewskiego 15, 93-590 Lodz, Poland. E-mail: brozek@mitr.p.lodz.pl*
[b]*Medical University of Lodz, Department of Pathology, Chair of Oncology, Paderewskiego 4, 93-509 Lodz, Poland. E-mail: j_proteus@wp.pl*
[c]*Medical University of Lodz, Department of Pathology, Chair of Oncology, Paderewskiego 4, 93-509 Lodz, Poland. E-mail: radzislaw.kordek@umed.lodz.pl*
[d]*WITec Wissenschaftliche, Instrumente und Technologie GmbH, Lise-Meitner-Str. 6, D-89081 Ulm, Germany. E-mail: elena.bailo@witec.de*
[e]*WITec Wissenschaftliche, Instrumente und Technologie GmbH, Lise-Meitner-Str. 6, D-89081 Ulm, Germany. E-mail: thomas.dieing@witec.de*
[f]*Lodz University of Technology, Institute of Applied Radiation Chemistry, Laboratory of Laser Molecular Spectroscopy, Wroblewskiego 15, 93-590 Lodz, Poland. E-mail: abramczy@mitr.p.lodz.pl*

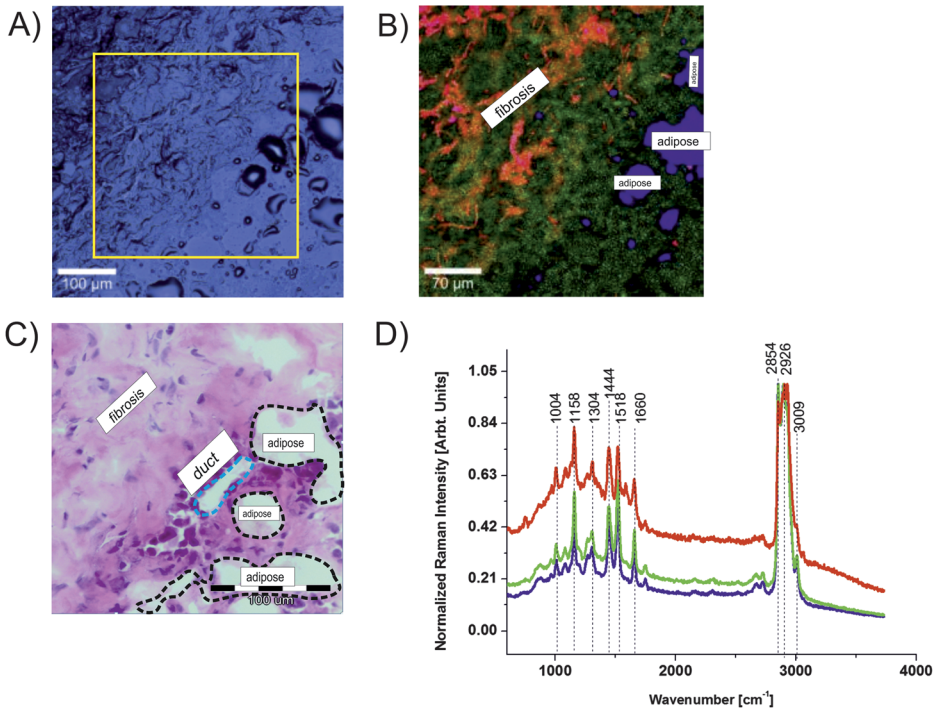

Fig. 1 Microscopy, Raman and histological images and Raman spectra of the noncancerous breast tissue of patient P80. (A) Microscopy image (500 × 500 µm) composed of several single video images of the noncancerous breast tissue, (B) Raman image (350 × 350 µm) of the cryosectioned noncancerous tissue from the region marked in (A) obtained by the basis analysis, (C) H&E stained histological image of the noncancerous breast tissue, and (D) Raman spectra of the noncancerous breast tissue. The colours of the Raman spectra correspond to the colours in the Raman image. Mixed areas are displayed as mixed colours. Integration time: 0.03 s.

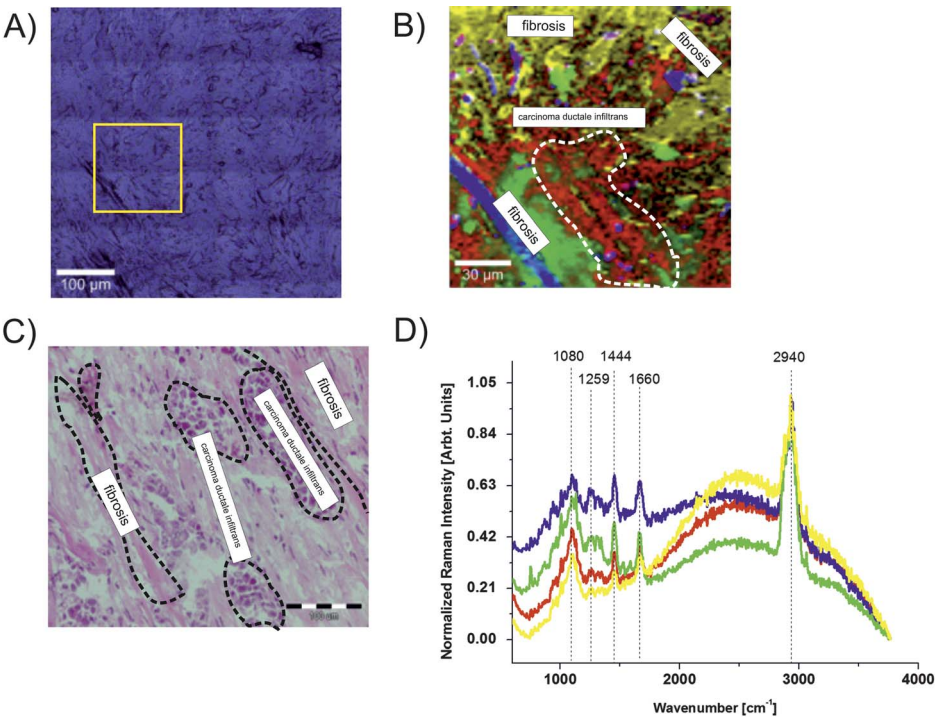

Fig. 2 Microscopy, Raman and histological images and Raman spectra of the cancerous breast tissue (infiltrating ductal cancer, G3) of the patient P80. (A) Microscopy image (500 × 500 µm) composed of several single video images of the cancerous breast tissue, (B) Raman image (150 × 150 µm) of the cancerous cryosectioned tissue from the region marked in (A) obtained by cluster analysis, (C) H&E stained histological image of the cancerous breast tissue, and (D) Raman spectra of the cancerous human breast tissue. The colours of the spectra correspond to the colours in the image. Mixed areas are displayed as mixed colours. Integration time: 0.03 s.

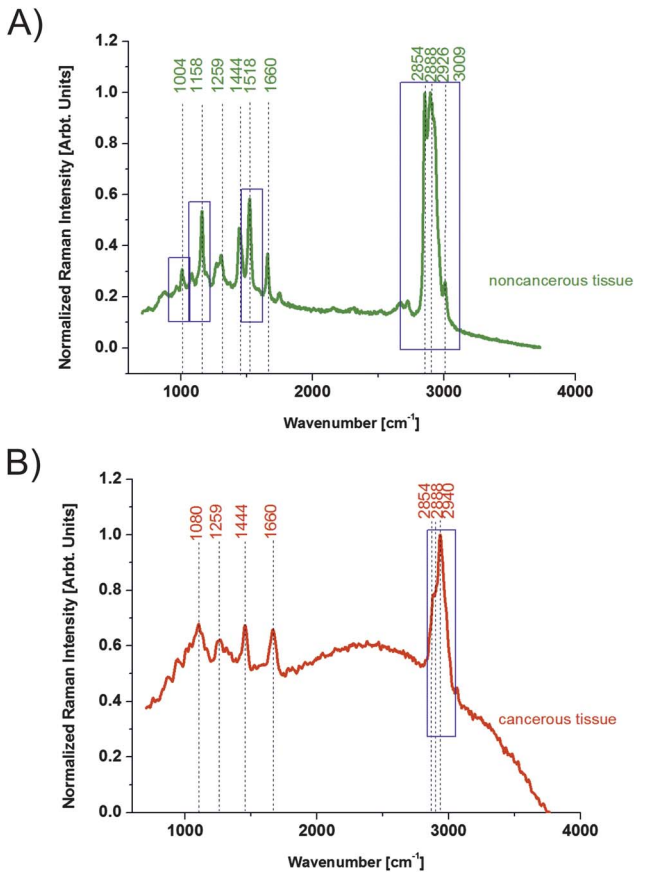

Fig. 3 Comparison of the Raman spectra of the noncancerous (A) and the cancerous (infiltrating ductal cancer, G3) (B) breast tissues of the same patient P80.

Results obtained by our group also confirm the huge potential of RS and RI in breast cancer diagnostics for excitation from the VIS range.[19–22]

The superiority of RS and RI over histological analysis results from several reasons: they can directly provide biochemical information concerning tissue composition, and they can monitor the tissue without any external agents and stains so that the overall time consumed is reduced and complicated preparation of samples is not needed. Moreover, novel technical solutions provide very high spatial resolution enabling the observation of the detailed cell anatomy.

From a practical point of view, what is especially important is the possibility to directly identify tumor markers based on biochemical information. A huge part of spectroscopic research is focused on the determination of such markers, which are formed in the human body as a response to the developing disease process.

The aim of the present study is to demonstrate that label-free RI has introduced the ability to accurately characterize breast cancer tissue and distinguish between noncancerous and cancerous types based on the endogenous vibrational markers.

The results presented in this paper provide evidence that the chemical composition of the tissue, especially in regions characteristic for carotenoids, lipids, and proteins in the noncancerous tissue, differs significantly from that of the cancerous tissue, and may represent a key factor responsible for mechanisms of carcinogenesis. Lipids are critical to all biological systems as they form biological membranes. Altered tumor cell lipid metabolism often means abnormal production of lipid transmitters of information and changes in the chemical composition of biological membranes. These changes may affect the location of enzymes involved in the synthesis and degradation of lipids and the expression of genes encoding these enzymes. It is well known that carotenoids naturally support the immune system as antioxidants, reduce DNA damage and support a healthy heart. Carotenoids also allow maintenance of a healthy cholesterol level and increase lung capacity.

2. Experimental methods

Patients and samples

In the described study, Raman spectroscopy and Raman imaging have been employed to analyze human breast cancer specimens. All procedures were conducted under a protocol approved by the Bioethical Committee at the Medical University of Lodz (RNN/29/11/KE/15/02/2011, RNN/30/11/KE/15/02/2011). We have studied samples of infiltrating ductal carcinoma, grade G3. Two types of samples were examined: a tissue sample from the tumor mass and tissue from the safety margins outside the tumor mass. All tissue samples were snap frozen and stored at −80 °C. One part of each type was cryosectioned with a microtome (Microm HM 550, Sermed) into 6 μm thick sections for Raman analysis. The thin cryosectioned tissue samples (without staining and paraffin embedding) have been examined by Raman imaging. After Raman analysis these sections were stained and histologically examined. The adjacent part of the tissue was paraffin embedded and also cut into 6 μm thick sections for histological analysis. The paraffin-embedded sections were put on microscopic glass slides, deparaffinized and stained with hematoxylin and eosin for histological diagnosis of the suspected areas. Two kinds of sample preparation have been used to check how the paraffin-embedding and deparaffinization procedures affect the Raman results and whether they interfere with essential indicators of the cancer pathology.

Unsaturated fatty acids

Unsaturated fatty acids, oleic acid (product number O1008), linoleic acid (product number L1367), α-linolenic acid (product number L2376), γ-linolenic acid (product number L2378), docosahexaenoic acid (product number D2534) and eicosapentaenoic acid (product number E2011), were purchased from Sigma-Aldrich and used without purification.

Instrumentation

All Raman images and spectra reported in this study were acquired using a Ramanor U1000 Raman spectrometer (Jobin Yvon) excited with an ion Ar laser (514 nm) and alpha 300 RA (WITec, Ulm, Germany) model consisting of a Zeiss microscope, coupled with a UHTS spectrometer and a Newton-EMCCD camera (operating in standard mode with 1600 × 200 pixels, at −64 °C with full vertical binning). The laser beam doubled

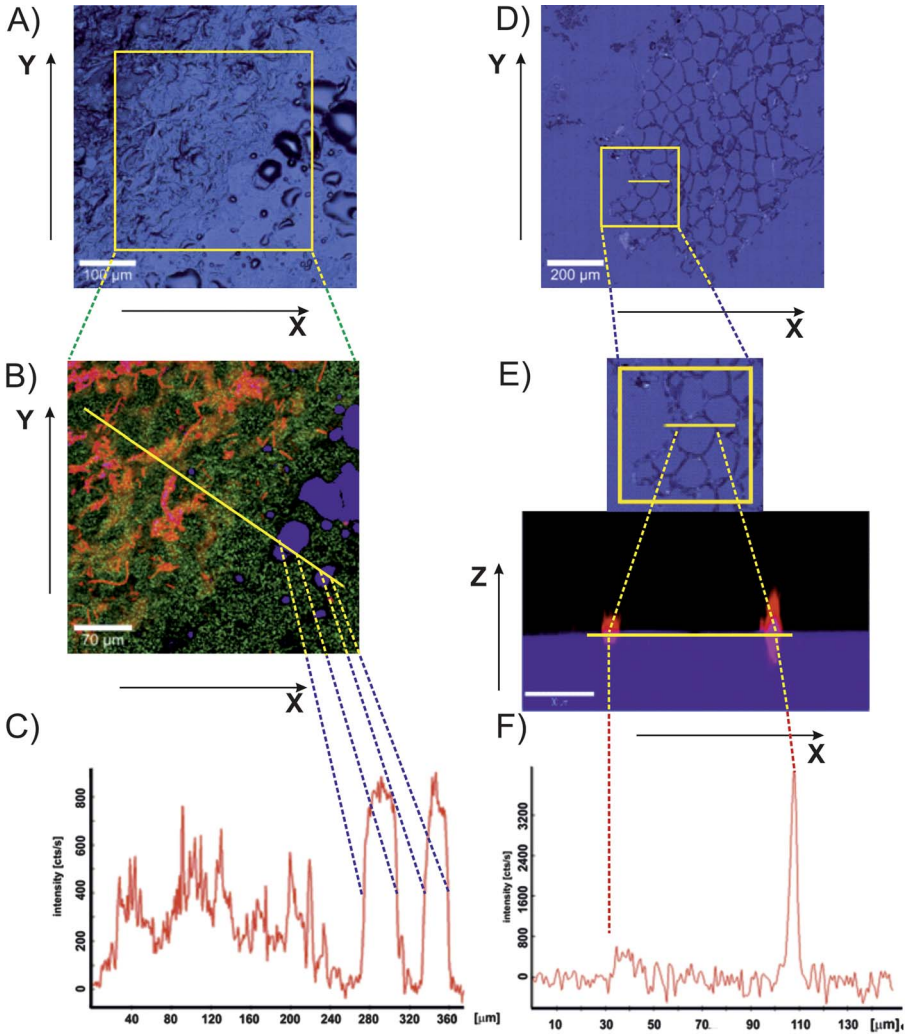

Fig. 4 Microscopy image (500 × 500 µm) composed of several single video images of the noncancerous breast tissue (A). Raman image (B) (350 × 350 µm) of the noncancerous breast tissue and the schematic representation (C) of CH bond intensity changes characteristic for lipids (2800–3000 cm^{-1}) along the cross line (the yellow line) shown in the Raman image of the cryosectioned specimen. The microscopy image composed of hundreds of video images of the sample (1000 × 1000 µm) (D). Raman image (E) (*x*: 150 µm; *z*: 50 µm), the schematic representation of CH bonds (2800–3000 cm^{-1}) intensity changes (F) along the cross line (the yellow line) shown in the stitching image (E) (1000 × 1000 µm) of the noncancerous breast tissue for the sample after deparaffinization of the same patient P80.

SHG of the Nd:YAG laser (532 nm) was focused on the sample with a 50× objective to the spot of 650 nm. The average laser intensity was 10 mW. Spectra were acquired using WITEC Project Plus software.

Data analysis method

2D arrays of thousands of individual Raman spectra were evaluated by basis analysis or the cluster method. In the basis analysis method each measured spectrum of the 2D spectral array is compared to the basis spectra using a least square fit. The basis spectra are created by averaging over various areas of the scanned surface or by using cluster analysis. The weight factor in each point is represented as a 2D image of the corresponding color and mixed coloring component. It tries to minimize the fitting error *D* described by eqn (1)

$$D = \left(\overrightarrow{[\text{recorded spectrum}]} - a \times \overrightarrow{\text{BS}_\text{A}} - b \times \overrightarrow{\text{BS}_\text{B}} - c \times \overrightarrow{\text{BS}_\text{C}} - \cdots\right)^2 \quad (1)$$

by varying the weighting factors *a*, *b*, *c*, … of the basis spectra $\overrightarrow{\text{BS}}$.[23]

In the presented paper the following steps were taken for each of the combined images using WITEC Project Plus software: background subtraction, cosmic ray removal, averaging a certain region manually, and spectral de-mixing. In the cluster analysis method Raman images are sorted according to their similarities. As a result one gets a certain number of areas or masks, which indicate where the spectra belonging to the various clusters were acquired as well as the average spectra of each cluster. The cluster analysis method has the advantage of being an automated and objective method to find similar regions in spectral datasets. It

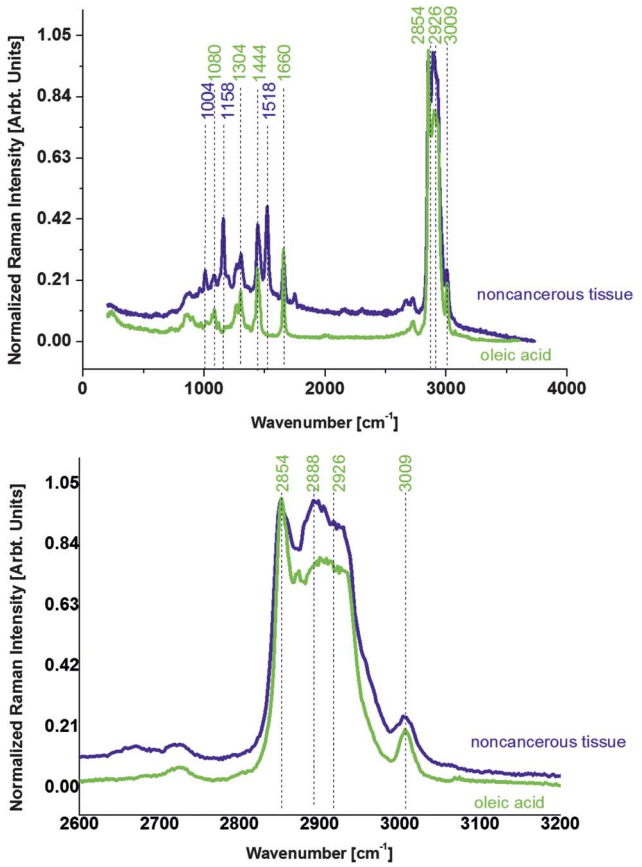

Fig. 5 Comparison of Raman spectra of the noncancerous breast tissue and oleic acid.

can however require significant processing power and time. In the presented paper spectral mapping was based on *K*-means cluster analysis.

3. Results and discussion

In this section, the results of the Raman studies on the noncancerous and the cancerous human breast tissues of the same patient are presented.

The typical Raman spectra of the noncancerous and the cancerous (infiltrating ductal cancer, G3) breast tissues are presented in Fig. 1 and 2.

Fig. 3 demonstrates comparison of the Raman spectra of the noncancerous and the cancerous (infiltrating ductal cancer, G3) breast tissues of the same patient.

One can see that the Raman spectra of the noncancerous and the cancerous breast tissues differ significantly in the regions characteristic for carotenoids and lipids. The Raman spectrum of the noncancerous tissue is dominated by the peaks at around 1004, 1158, 1259, 1444, 1660, 2854, 2888, and 2926 cm^{-1}, while the spectrum of the cancerous tissue shows characteristic peaks at around 1080, 1259, 1444, 1660, 2888, and 2940 cm^{-1}.

The peaks at 1004, 1158, and 1518 cm^{-1} of the noncancerous tissue correspond to vibrations typical for the C–C and C=C stretching modes of carotenoids, and the peak at 1259 cm^{-1} corresponds to the asymmetric stretching mode of the PO_2^- group. Other apparent vibrations characteristic for the C–H groups of lipids are 1444 (scissoring mode), 1660 (C=C stretching mode), 2854 (symmetric stretching mode), 2888 (stretching mode), and 2926 cm^{-1} (asymmetric stretching mode), and the peak at 3009 cm^{-1} corresponds to the (C=C)–C–H asymmetric stretching mode. The cancerous breast tissue shows strong peaks at 1080, 1259, 1444, 1660, 2854, and 2940 cm^{-1}, the peak at 1080 cm^{-1} corresponds to phospholipids, and the vibrations at 2854 cm^{-1} are typical for the CH group of lipids, while the vibrations at 2940 cm^{-1} can be defined as a combination of the vibrations of lipids and proteins.[24–29]

In summary, the detailed description of the characteristic peaks of the cancerous and the noncancerous breast tissues confirms that the pronounced differences between these types of tissues can be seen in the regions typical for lipid, carotenoid and protein vibrations.

Having reached a point where it is possible to suggest which vibrations are preferentially monitored by Raman spectroscopy in the normal and the cancerous tissues, it is important to check how the preparation of the tissue may change Raman features. Comparison of the lipid profile of the cryosectioned specimens and the histological samples after deparaffinization has been performed. Fig. 4 shows the comparison of the Raman images of the cryosectioned sample and the sample after deparaffinization of the same patient P80.

Fig. 4A presents the microscopy image of the noncancerous tissue prepared by cryosectioning and Fig. 4B presents the Raman image of the same sample as in Fig. 4A. Fig. 4C shows the distribution of lipids and proteins along the yellow cross line as marked in Fig. 4B. Lipids and proteins are monitored *via* the filter (region 2800–3000 cm^{-1}), which contains the characteristic CH vibrations of these compounds. One can see from Fig. 4C that the most intense and broad peaks correspond to adipose cells (blue areas in Fig. 4B). Fig. 4D–F present the results for the same patient but the thin sections were obtained from deparaffinization, not from cryosectioning. From comparison of Fig. 4C and F one can notice significantly different distribution of lipids and proteins after deparaffinization demonstrated by only two visible peaks in contrast to the results from Fig. 4C. These peaks correspond to the points where the yellow line crosses the cell membrane (Fig. 4D and E). One can see from Fig. 4F that there is no Raman signal from the intracellular area. It indicates that the lipid fraction contained in the adipose cell is washed out during the deparaffinization procedure. Therefore, the paraffin-embedding and deparaffinization procedures should be avoided for Raman measurements, because they wash out fatty acids, which may be important indicators of cancer pathology.

A detailed inspection of Fig. 3 shows that the vibrations characteristic for carotenoids and lipids play a leading role in distinguishing between cancerous and noncancerous human breast tissues and can be determined as Raman biomarkers for molecular diagnostics.

Carotenoids, represented in the Raman spectra of the noncancerous tissue by the peaks at 1004, 1158, and 1518 cm^{-1}, are well known as natural antioxidants that can neutralize reactive oxygen species and can reduce oxidative DNA damage and genetic mutations. Carotenoids can also enhance certain immunologic functions of human organisms. All these functions

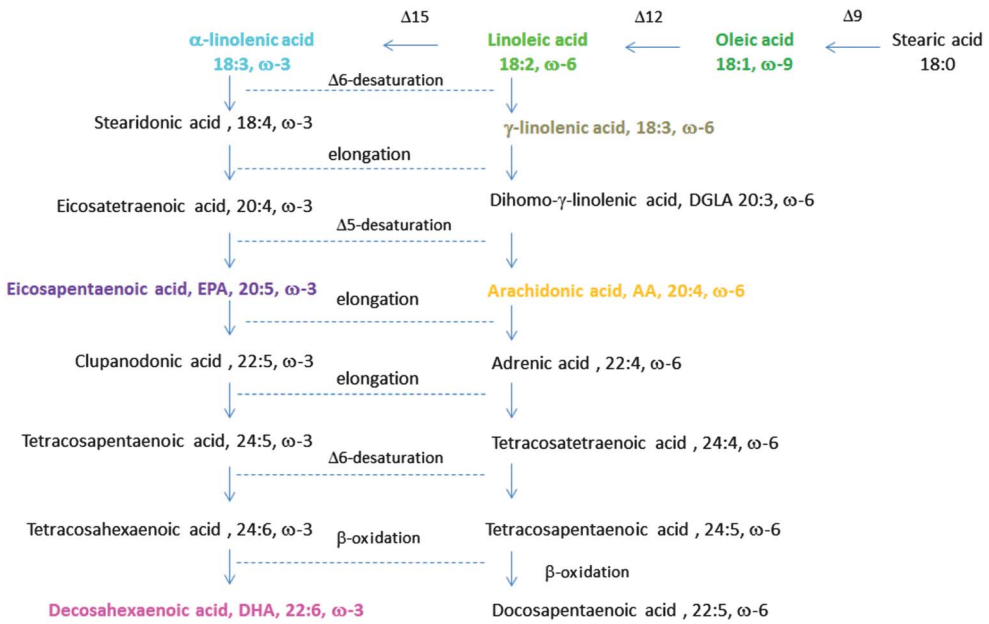

Scheme 1 Schematic presentation of the fatty acid metabolism.

of carotenoids can act as a protective factor against breast cancer.[30–32]

A detailed inspection of Fig. 3 and 4 shows also the crucial role played by the lipid vibrations in distinguishing between noncancerous and cancerous breast tissues. The lipid profile in the region around 2800–3200 cm^{-1} is evidently different for the noncancerous and the cancerous tissues with an additional component at 2940 cm^{-1} corresponding to proteins in the latter. Our study proves that the profile typical for the noncancerous tissue is dominated by oleic acid (Fig. 5).[20]

Oleic acid is a monounsaturated ω-9 fatty acid found in various animal and vegetable fats, and what is relevant to this study is that it is also a parent acid of many unsaturated acids like linoleic acid (LA), α-linolenic acid (ALA), eicosapentaenoic acid (EPA), and docosahexaenoic acid (DHA) from the ω-3 family, and γ-linolenic acid (GLA), dihomo-γ-linolenic acid (DGLA) and arachidonic acid (AA) from the ω-6 family of acids. Scheme 1 presents the fatty acid metabolism.

Polyunsaturated fatty acids play an important role in human organisms, being precursors of eicosanoids which are known to be tissue hormones. These compounds are very unstable and hence rapidly decompose and can act as a factor triggering cancer. These compounds include prostaglandin (PG), prostacyclin (PGI) and thromboxanes (TX), known together as prostanoids and leukotrienes (LT).[33]

Eicosanoid precursors are DGLA, AA and EPA. As a result of phospholipase A_2 action they are released from phospholipid cell membranes. The cyclooxygenase (COX) catalyzes the synthesis of cyclic compounds – PG, PGI, and TX, while the lipoxygenase (LOX) catalyzes the synthesis of noncyclic compounds. The type and amount of the synthesized eicosanoids are dependent on the availability of the precursor and the activity of phospholipase A_2, phospholipase C, cyclooxygenase and lipoxygenase. Frequently AA is a precursor of eicosanoids and their derivatives which have a much higher biological activity than the derivatives of DGLA and EPA, even in very small quantities. Eicosanoids produced *via* AA metabolism stimulate the development of atherosclerosis, thrombus formation, severe inflammation and allergic reactions, as well as cell proliferation and growth of tumor tissue, especially in the mammary gland, colon and prostate.[34–36] The important role of fatty acids described above prompted us to investigate the spectroscopic properties of this class of compounds. We have recorded Raman spectra of LA, ALA, DHA, EPA, GLA and AA and compared them with the cancerous and noncancerous breast tissues. The results are presented in Fig. 6.

One can see from Fig. 5 and 6 that the Raman spectrum of the noncancerous breast tissue is well reproduced by the spectra of oleic acid (OA) and linoleic acid (LA); some similarities with docosahexaenoic acid (DHA) can also be found. DHA is the precursor of eicosanoids that are less inflammatory when compared to AA prostanoids. The protective roles of OA, DHA and carotenoids in breast cancer risk have been proved in clinical trials.[37,38] A surprising result has been obtained for eicosapentaenoic acid (EPA). The Raman spectrum of EPA in the region 2800–3200 cm^{-1} did not reproduce the profile of the noncancerous breast tissue in a considerable scope, even though EPA is considered as a factor lowering the risk of breast cancer.[39]

In contrast the profile of the cancerous breast tissue presented in Fig. 6 is more similar to the spectra of γ-linolenic acid (GLA) and arachidonic acid (AA), which play a central role in injury and many diseased states. Potential mechanisms of these ω-6 acids in promoting cancer development are through the production of proinflammatory eicosanoids such as prostaglandin E2, which promotes angiogenesis and hinders apoptosis.[40] AA influences human health and the *in vitro* activity of immune cells. Moreover, AA is very susceptible to lipid peroxidation. *In vitro* studies have shown that the secondary products of lipid peroxidation suppress mammary tumorigenic processes by causing an increased accumulation of these cytotoxic or cytostatic products in tumor tissue[41] or by creating intermolecular linkages, intramolecular linkages, or both, between amino acid sulfhydryl groups of RNA, DNA, and

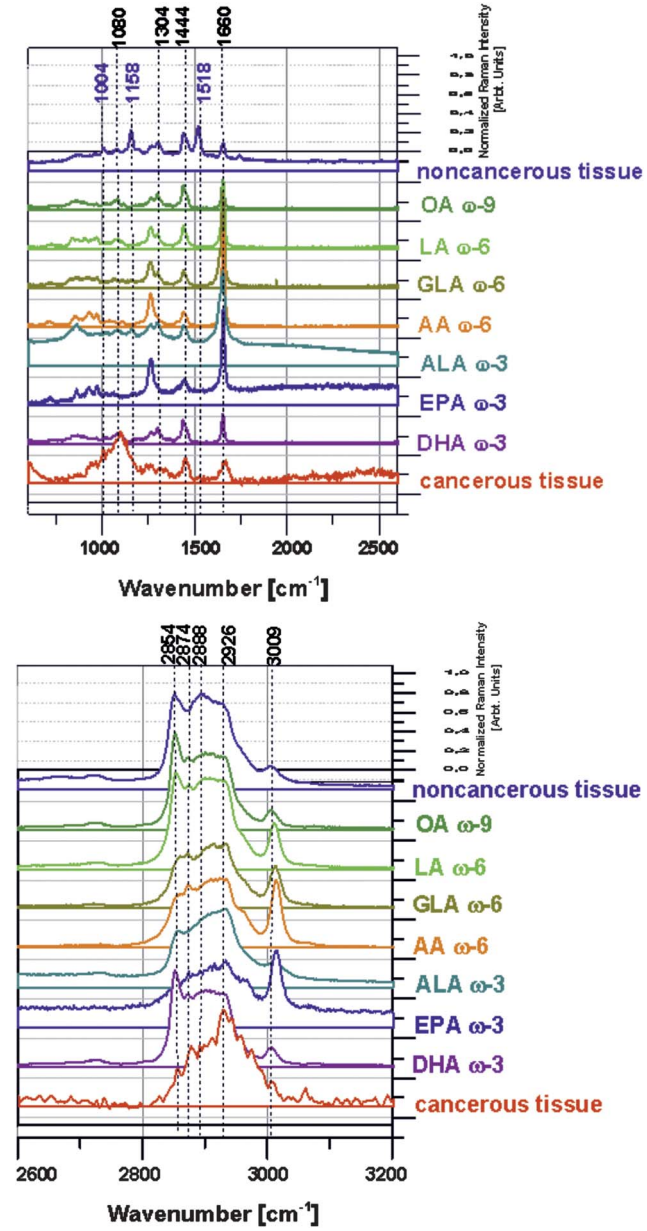

Fig. 6 Comparison of Raman spectra of the noncancerous and the cancerous (infiltrating ductal carcinoma, G3) breast tissues of patient P80 and oleic acid (OA), linoleic acid (LA), γ-linolenic acid (GLA), arachidonic acid (AA), α-linolenic acid (ALA), eicosapentaenoic acid (EPA) and, docosahexaenoic acid (DHA).

proteins, which leads to the inactivation or damage of these molecules.[41–43]

The main difficulty in interpretation of the bands in the region of 2800–3000 cm^{-1} comes from the fact that the location of bands in the Raman spectra of fatty acids in lipids overlap with the bands of proteins. The main protein band near 2940 cm^{-1} attributed to aromatic and aliphatic amino acids and many other amino acids overlap with the band of fatty acids.

Even if the cancerous human breast tissue shows some similarities with the Raman spectra of the ω-6 acids such as GLA and AA one can notice the lack of the band at 3009 cm^{-1} in the cancerous tissue in contrast to GLA and AA, where the band is

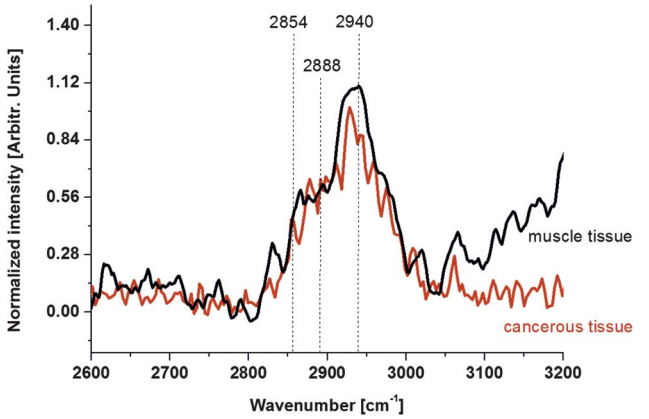

Fig. 7 Comparison of the Raman spectrum of the cancerous tissue and the spectrum of an animal muscle tissue.

clearly visible. It may simply indicate that the band at around 2800–3000 cm^{-1} is dominated by proteins rather than fatty acids.

Fig. 7 shows the comparison of the Raman spectrum of the cancerous breast tissue of the same patient as in Fig. 5 and 6 with the spectrum of an animal muscle tissue.

One can see from Fig. 7 that the profile of the cancerous tissue is very similar to the protein component. It is well known[44,45] that high protein production is linked to cell division, migration and increased cell proliferation in tumors. It has been shown that high levels of proteins are also present in breast cancer specimens and cell lines. The growing contribution from the protein components from the beginning of cancer research has been indicated as a characteristic of carcinogenesis.[14,15] Approximately 30% of breast cancers have an amplification of the HER2/neu gene or overexpression of its protein product.[46]

In summary, we have shown that carotenoids, fatty acid content, and lipid profile, as well as the protein amount in cancerous and noncancerous human breast tissues, are significantly different. It remains a question whether the differences could have an impact on the activity of the processes that drive the transformation into the pathology, or if they are the consequence of a different hormonal milieu in the normal and cancerous tissues.

4. Conclusions

The presented paper has illustrated important aspects of the Raman vibrational features of human breast tissue. The typical Raman spectra and Raman images of the cancerous human breast tissue of a patient suffering from infiltrating ductal carcinoma and noncancerous tissue from the safety margin surrounding the tumor mass have been presented. Evidence has been provided that the deparaffinization protocol distorts the lipid profile of the breast tissue and must be eliminated in the process of sample preparation for Raman diagnostics.

The results presented in this study demonstrate that Raman spectra and images are sensitive indicators of distribution of lipids, proteins, and carotenoids in breast tissue.

Comparison of Raman spectra of breast tissue indicates that the Raman spectrum of the cancerous tissue seems to be dominated by the protein component while the spectra of

noncancerous tissue seem to be more similar to the spectra of oleic acid and ω-3 acids (LA, ALA and DHA).

The fatty acid metabolism products monitored and identified by Raman spectroscopy in the cancerous breast tissue may be related to important mechanisms involved in carcinogenesis.

Carotenoids and fatty acids can be treated as Raman biomarkers to distinguish between cancerous and noncancerous human breast tissues.

Acknowledgements

We would like to express our gratitude toward the support of this work through the grants: 2940/B/T02/2011/40 funded by The National Science Centre, the grant 3845/B/T02/2009/37 of the Ministry of Science and Higher Education and the Dz. St 2012. We would like to thank Witec Company and Dr Jan Toporski for the fruitful collaboration in confocal Raman microscopy measurements.

References

1 S. Lee, H. Chon, M. Lee, J. Choo, S. Y. Shin, Y. H. Lee, I. J. Rhyu, S. W. Son and C. H. Oh, *Biosens. Bioelectron.*, 2009, **24**, 2260–2263.
2 P. Lasch and D. Nauman, *Biochim. Biophys. Acta*, 2006, **1758**, 814–829.
3 A. Kretlow, Q. Wan, J. Kneipp, P. Lasch, M. Beekes, L. Miller and D. Naumann, *Biochim. Biophys. Acta*, 2006, **1758**, 948–959.
4 P. Lasch, W. Haensch, D. Naumann and M. Diem, *Biochim. Biophys. Acta*, 2004, **1688**, 176–186.
5 A. Mahadevan-Jansen and R. Richards-Kortum, *Proc. IEEE/EMBS*, 1997, 2722–2728.
6 J. Kneipp, T. Bakker Schut, M. Kliffen, M. Menke-Pluijmers and G. Puppels, *Vib. Spectrosc.*, 2003, **32**, 67–74.
7 A. J. Berger, T. W. Koo, I. Itzkan, G. Horowitz and M. S. Feld, *Appl. Opt.*, 1999, **38**, 2916–2926.
8 K. Virkler and I. K. Lednev, *Anal. Bioanal. Chem.*, 2010, **396**, 525–534.
9 T. R. Hata, T. A. Scholz, I. V. Ermakov, R. W. McClane, F. Khachik, W. Gellermann and L. K. Pershing, *J. Invest. Dermatol.*, 2000, **115**, 441–448.
10 C. D. Sudworth, J. K. Archer and D. Mann, *Optical Spectroscopy in Biomedicine III*, ed. A. Mycek, Proc. SPIE, Optical Society of America, 2005, vol. 5862, TuC3.
11 R. J. Swain and M. M. Stevens, *Biochem. Soc. Trans.*, 2007, **35**, 544–549.
12 M. Hedegaard, Ch. Krafft, H. J. Ditzel, L. E. Johansen, S. Hassing and J. Popp, *Anal. Chem.*, 2010, **82**, 2797–2802.
13 K. E. Shafer-Peltier, A. S. Haka, J. T. Motz, M. Fitzmaurice, R. R. Dasari and M. S. Feld, *J. Cell. Biochem.*, 2002, **87**, S125–S137.
14 R. R. Alfano, C. H. Liu, W. L. Sha, H. R. Zhu, D. L. Akins, J. Cleary, R. Prudente and E. Cellmer, *Laser. Life Sci.*, 1991, **4**, 23–28.
15 D. C. Redd, Z. C. Feng, K. T. Yue and T. Gansler, *Appl. Spectrosc.*, 1993, **47**, 787–791.
16 A. S. Haka, K. E. Shafer-Peltier, M. Fitzmaurice, J. Crowe, R. R. Dasari and M. S. Feld, *Proc. Natl. Acad. Sci. U. S. A.*, 2005, **102**, 12371–12376.
17 N. Stone and P. Matousek, *Cancer Res.*, 2008, **68**(11), 4424–4430.
18 N. Stone, C. Kendall, J. Smith, P. Crow and H. Barr, *Faraday Discuss.*, 2004, **126**, 141–183.
19 H. Abramczyk, J. Surmacki, B. Brozek-Pluska, Z. Morawiec and M. Tazbir, *J. Mol. Struct.*, 2009, **924–926**, 175–182.
20 H. Abramczyk, B. Brozek-Pluska, J. Surmacki, J. Jablonska-Gajewicz and R. Kordek, *Prog. Biophys. Mol. Biol.*, 2012, **108**, 74–81.
21 B. Brożek-Płuska, I. Placek, K. Kurczewski, Z. Morawiec, M. Tazbir and H. Abramczy, *J. Mol. Liq.*, 2008, **141**, 145–148.
22 B. Brozek-Pluska, J. Jablonska-Gajewicz, R. Kordek and H. Abramczyk, *J. Med. Chem.*, 2011, **54**, 3386–3392.
23 T. Dieing, O. Hollricher and J. Toporski, *Confocal Raman spectroscopy*, Springer-Verlag, Berlin Heidelberg, 2010.
24 P. Lash and D. Naumann, *Biochim. Biophys. Acta*, 2006, **1758**, 814–829.
25 H. Fabian, N. A. N. Thi, M. Eiden, P. Lash, J. Schmitt and D. Naumann, *Biochim. Biophys. Acta*, 2006, **1758**, 874–882.
26 P. Lasch, A. Pacifico and M. Diem, *Biopolymers*, 2002, **67**, 335–338.
27 L. M. Miller and P. Dumas, *Biochim. Biophys. Acta*, 2006, **1758**, 846–857.
28 L. M. Miller, P. Dumas, N. Jamin, J. L. Teillaud, J. L. Bantignies and G. L. Carr, *Inst. Of Physics Conf. Series sponsored by Micro Beam Analysis*, 2000, vol. 165, pp. 75–76.
29 E. Gazi, P. Gardner, N. P. Lockyer, C. A. Hart, N. W. Clarke and M. D. Brown, *J. Lipid Res.*, 2007, **48**, 1846–1856.
30 P. Toniolo, A. L. Van Kappel, A. Akhmedkhanov, P. Ferrari, I. Kato, R. E. Shore and E. Riboli, *Am. J. Epidemiol.*, 2001, **153**, 1142–1147.
31 K. Rahman, *Clin. Interventions Aging*, 2007, **2**(2), 219–236.
32 M. R. McCall and B. Frei, *Free Radical Biol. Med.*, 1999, **26**(7–8), 1034–1053.
33 L. Zhou and Å. Nilsson, *J. Lipid Res.*, 2001, **42**, 1521–1542.
34 P. Benatti, G. Peluso, R. Nicolai and M. Calvani, *J. Am. Coll. Nutr.*, 2004, **23**, 281–302.
35 A. C. Shapir, D. Wu and S. N. Meydani, *Prostaglandins*, 1993, **45**, 229–240.
36 M. L'Hirondel, A. Cheramy, G. Godeheu and J. Glowinski, *J. Neurochem.*, 1995, **64**, 1406–1409.
37 A. Nkondjock and P. Ghadirian, *Canada. Am. J. Clin. Nutr.*, 2004, **79**, 857–864.
38 J. A. Menendez, L. Vellon, R. Colomer and R. Lupu, *Ann. Oncol.*, 2010, **16**, 359–371.
39 E. A. de Deckere, *Eur. J. Cancer Prev.*, 1999, **8**, 213–221.
40 H. Tapiero and G. N. Ba, *Biomed. Pharmacother.*, 2002, **56**, 215–222.
41 M. J. Gonzalez, R. A. Schemmel, J. I. Gray, L. Dugan, L. G. Sheffield Jr and C. W. Welsch, *Carcinogenesis*, 1991, **12**, 1231–1235.
42 U. Reiss and A. L. Tappel, *Lipids*, 1973, **8**, 199–202.
43 L. C. Hamilton, J. A. Mitchel, A. M. Tomlinso and T. D. Warner, *FASEB J.*, 1999, **13**, 245–251.
44 V. Baeten, M. Morales and R. Aparicio, *J. Agric. Food Chem.*, 1999, **47**, 2225–2230.
45 V. Baeten and R. Aparicio, *Biotechnol., Agron., Soc. Environ.*, 2000, **4**, 196–203.
46 M. A. Olayioye, *BreastCancer Res.*, 2001, **3**(6), 385–389.

